Charge-Doped and Heteroatom-Substituted Polysilane, Poly(vinylenedisilanylene), and Poly(butadienylenedisilanylene): Electronic Structures and Band Gaps

Guiling Zhang,[†,‡] Jing Ma,[*,†] and Yuansheng Jiang[†]

Department of Chemistry, Institute of Theoretical and Computational Chemistry, Key Lab of Mesoscopic Chemistry of MOE, Nanjing University, Nanjing 210093, P. R. China, and Department of Chemistry, Harbin Normal University, Harbin 150080, P. R. China

Received: March 11, 2005; In Final Form: May 13, 2005

The effects of charge-doping and boron and phosphorus substitution on the electronic structures and band gaps of polysilane, poly(vinylenedisilanylene), and poly(butadienylenedisilanylene) were theoretically investigated by using density functional theory and time-dependent density functional theory. Band gaps of polymers were estimated both by extrapolations from excitation energies of oligomers up to 30 units and by calculations with the periodic boundary condition. It was found that charge-doping in the polysilane decreases the band gap more significantly than B and P substitutions. However, Si−Si bonds are easily broken by charge-doping. In contrast, B and P substitutions exert little influence on the strength of Si−Si bonds. From natural bond orbital analysis, it was concluded that charge-doping and heteroatom substitution bring about a lowering of the band gap in σ conjugated polysilanes because of strong electron−hole interactions. The introduction of longer π conjugated moieties was found to reduce band gaps of $\sigma-\pi$ conjugated chains. In contrast to the σ conjugated polysilanes, bridged structures and a different distribution of polarons were found in cations of $\sigma-\pi$ conjugated chains.

1. Introduction

One-dimensional σ and $\sigma-\pi$ conjugated chains such as polysilane [**PSi**, $-(SiH_2)_n-$], poly(vinylenedisilanylene) [**PVD**, $-(SiH_2SiH_2CH{=}CH)_n-$], and poly(butadienylenedisilanylene) [**PBD**, $-(SiH_2SiH_2CH{=}CH{-}CH{=}CH)_n-$] are of growing interest because they exhibit semiconductivity, photoconductivity, and electroluminescence.[1] Most interestingly, these materials have been demonstrated to function as nanowires.[2] The properties of these polymers are related to the relative amounts of σ or $\sigma-\pi$ conjugation in their backbones. As in the case of π conjugated polymers,[3] introduction of entities called polarons or bipolarons by physicists[4] (ion-radicals or biradicals in the language of chemists[5]) into the σ and $\sigma-\pi$ conjugated chains is an effective way to lower their band gaps, E_g, to the point that they become semiconductors or even conductors.[1c,e] Charge-doping and heteroatom substitution of the silicon atom are two effective techniques for obtaining polaronized σ and $\sigma-\pi$ conjugated oligomers and polymers. Therefore, the investigation of electronic structures and band gaps of charged and substituted σ and $\sigma-\pi$ conjugated oligomers and polymers is of interest.

The charge-doping of oligosilanes (***n*Si**) and polysilanes (**PSi**) has been experimentally studied recently. From absorption spectra it was concluded that the excitation energies of radical cations and anions of oligosilanes decrease monotonically with increasing chain length.[6,7] Polarons and bipolarons are thought to function as charge carriers (whose distributions are related to the conductivities of polymers). From ESR spectra of radical ions of poly(cyclohexylmethylsilane)s it was derived that the polaron localized over a range of about six silicon atoms.[7] But a different conclusion was drawn from the electronic absorption spectra of the radical ions; in that case it was found that the polaron spreads over a region of 16 silicon atoms in the main chain of the poly(methyl-*n*-propylsilane).[6] The difference in those conclusions calls for theoretical investigations. In contrast to those of charged π conjugated chains, Si−Si bonds of the charged **PSi** are easily broken, as demonstrated by experiments.[1c] Moreover, the positively charged polaron in **PSi** (lifetimes of 30−100 μs) was suggested to be more stable than the negatively charged one (lifetimes of 5−30 μs).[8] This attracts our attention to the positive-charge-doping effects on oligosilanes and polysilanes. On the other hand, theoretical studies have provided some useful information on geometries and properties of singly charged oligosilanes.[9] MP4SDTQ/DZPD//MP2/DZPD[9a] and B3LYP/6-31G*[9b,c] results showed a lengthening of Si−Si bonds in radical anions and cations, ***n*Si**$^{\pm}$ ($n = 2-10$), relative to those in neutral ***n*Si** ($n = 2-10$), in line with the experimental observations.[1c] The first dipole-allowed excitation energies of charged oligosilanes have also been calculated by CIS[9a] and semiempirical PM3-CI[10] methods, from which a remarkable decrease in excitation energies compared with neutral oligosilanes was exhibited. Excitation energies were also predicted to simultaneously decrease with increasing chain length,[9a,10] in agreement with the experimental results.[6,7,11] However, it is still unclear what intrinsic factors lead to a lowering of excitation energies (and band gaps) of oligosilanes (and polysilanes) by charge-doping. Furthermore, there are still few studies concerning the relative stabilities and electronic structures of heavily oxidative oligosilanes and polysilanes such as dications.

Recently, boron and phosphorus have been successfully introduced into silicon nanowires controllably and have increased the conductivities of nanowires over many orders of magnitude.[2d] More encouragingly, geometry defects induced by boron and phosphorus were found to be sufficiently small that they could not break the nanowire into small islands. But the distribution of B and P atoms in nanowires has not been

† Nanjing University.
‡ Harbin Normal University.

10.1021/jp051259c CCC: $30.25
Published on Web 06/23/2005

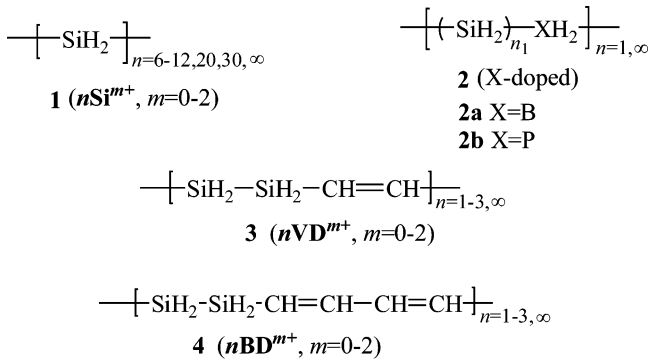

Figure 1. Selected chains for studying the charge-doping and heteroatom substitution effects on σ and $\sigma-\pi$ conjugated oligomers.

characterized yet. There is a possibility that B and P atoms may substitute silicon atoms, stimulating our interest in B- and P-substituted silicon chains. It has also been demonstrated that introduction of boron and phosphorus atoms yields p-type (holes) and n-type (electrons) semiconductors, respectively. However, the influence of heteroatoms in silicon nanowires is still unknown. *Are there any similarities between heteroatom substitution and charge-doping? If they are different, what is the difference between them?* The present comparative study of heteroatom substitution and charge-doping effects on the electronic structures and band gaps of polysilanes attempts to offer clues to answer these questions.

In addition, $\sigma-\pi$ conjugated systems with a regularly alternating arrangement of a disilanylene unit and a π-electron moiety such as vinylene, ethynylene, and thienylene have been synthesized, displaying conductivities in a range of $10^{-4}-10^{-1}$ S cm^{-1} after being doped with strong electron acceptors such as SbF_5 and AsF_5.[12] To enrich our knowledge of the structures and band gaps of charged $\sigma-\pi$ conjugated chains, more theoretical studies are desired. The difference between σ and $\sigma-\pi$ conjugations is hence expected to be unveiled.

Since the ultimate goal is to search for stable polaronized polymers with narrow band gaps, in this contribution our efforts are devoted to a systematic study on the effects of charge-doping and heteroatom substitution on the structures and band gaps of σ and $\sigma-\pi$ conjugated chains with broad molecular scales from oligomers (with 6−30 units) to polymers. The main topics addressed in the present work are (1) why heteroatom-substituted polymers are more stable than charged ones; (2) how charge-doping and heteroatom substitution reduce band gaps of σ and $\sigma-\pi$ conjugated polymers; and (3) the trend of changes in electronic structures and band gaps from lightly to heavily charged polysilanes.

2. Computational Details

Four series of σ and $\sigma-\pi$ conjugated chains, **1**−**4**, as shown in Figure 1, are selected in our study. As mentioned in the Introduction, the present study, covering a broad scope of both oligomers with up to 30 units and polymers, demands different theoretical models.

2.1. Calculations of Oligomers. Geometry optimizations and calculations of excitation energies of oligomers are performed using density functional theory (DFT) implemented in the Gaussian 98 program package.[13] Since calculations on doped oligomers (e.g., ***n*Si**$^+$) with unpaired electrons are sensitive to the choice of functionals,[14] we have performed extensive validation calculations on the geometries of ground states and the first dipole-allowed excitation energies with various functionals and basis sets (cf. Table 1), from which the BH&HLYP/6-31+G* level is selected for our further studies on oligomers **1**−**4**.

Radical Cations. It is widely recognized that electronic structures of singlet ground states of biradicals as well as long oligomers with biradical characters can be reasonably described by the broken-symmetry unrestricted DFT (BS-UDFT) method.[14b,15] This strategy is also employed in this work to calculate singlet states of neutral and doubly charged chains. To eliminate spin contaminations involved in unrestricted wave functions, we use formula (1), proposed by Yamaguchi et al.,[16] to correct the energy difference between singlet and triplet states, $\Delta E_{ST} = E_S - E_T$.

$$\Delta E_{ST} = \frac{E_{BS} - E_T}{\langle S^2\rangle_T - \langle S^2\rangle_{BS}}\langle S^2\rangle_T \qquad (1)$$

where E_{BS} and E_T are the total energies of broken-symmetry singlet states and the corresponding triplet states, respectively. $\langle S^2\rangle_T$ and $\langle S^2\rangle_{BS}$ denote the expectation values of the square of total spin angular momentum for triplet states and broken-symmetry singlet states, respectively.

Reasonable descriptions of radicals require the admixture of Becke exchange functional (BLYP) with HF exchange, because long-range correlation effects that keep interacting centers apart are overestimated by pure DFT exchange functionals. B3LYP and BH&HLYP are two extensively tested hybrid functionals with 20% and 50% HF exchange, respectively. To decide which is more suitable for calculations on selected radical cations of oligomers, we compared spin densities (an important feature of radicals) of silicon atoms of **30Si**$^+$ obtained by B3LYP/6-31+G* and BH&HLYP/6-31+G* optimizations, respectively (cf. Figure S1 in the Supporting Information). The distribution of spin densities obtained by BH&HLYP/6-31+G* indicates that radical (unpaired) electron can spread over a region of around 16 silicon atoms, in good agreement with experimental results (as mentioned in the Introduction).[6] The B3LYP/6-31+G* result shows a more even distribution of α-spin electron, with radical electron delocalizing all over the backbone of **30Si**$^+$. To verify that BH&HLYP/6-31+G* is appropriate for describing other properties, we did further validations as presented below.

Geometries. We selected **2Si**, **6Si**$^+$, and vinyldisilane (**VD**) to test the influence of basis sets on optimized geometries (Table 1). Bond lengths of **2Si**, **6Si**$^+$, and **VD** obtained from the 6-31+G* basis set are in good agreement with experimental data[1d] and those obtained from higher basis sets (6-31+G** and 6-311+G**). In addition, there is little difference in optimized geometries between BH&HLYP/6-31+G* and other methods, such as MP2/6-31+G* and B3LYP/6-31+G*. Therefore, it is feasible to employ BH&HLYP/6-31+G* to optimize the geometries of σ and $\sigma-\pi$ conjugated oligomers.

Excitation Energies. TDDFT calculations on vertical excitation energies were performed at optimized geometries of ground states with the 6-31+G* basis set. Table 1 also lists the excitation energies of **2Si**, **6Si**$^+$, and **VD**, from which we can find that the TDDFT excitation energy of **2Si** obtained from BH&HLYP/6-31+G* is in better agreement with experimental data[17] (with a variance of 0.18 eV) than that obtained from B3LYP/6-31+G* (with a variance of 0.41 eV). As shown in Table 1, moreover, there is a negligible difference of less than 0.05 eV in TDDFT/BH&HLYP excitation energies of studied species between the 6-31+G* basis set and larger basis sets (6-31+G** and 6-311+G**). Since in the present work we are

TABLE 1: Validations for BH&HLYP/6-31+G* Calculations on Oligomers and PBC/PW91 Studies on Polymers by Comparison with Results from Experiments and Other Methods (TDDFT Calculations on Excitation Energies of Oligomers Are Carried Out at the Optimized Geometry with BH&HLYP/6-31+G*)

		bond lengths of oligomers/Å					
		2Si	**6Si**$^{+b}$		**VD**^{c}		
method	basis set	R_{SiSi}	R_{SiSi}	$\overline{R_{SiSi}}$	R_{SiSi}	R_{SiC}	R_{CC}
Exp.[a]		2.32					
BH&HLYP	6-31G	2.36	2.44	2.42	2.36	1.89	1.33
	6-31G*	2.34	2.39	2.38	2.34	1.87	1.33
	6-31+G*	2.34	2.40	2.39	2.35	1.87	1.33
	6-31+G**	2.34	2.40	2.39	2.35	1.87	1.33
	6-311+G**	2.34	2.40	2.39	2.35	1.87	1.33
B3LYP	6-31+G*	2.35	2.40	2.40	2.36	1.88	1.34
BLYP	6-31+G*	2.37	2.42	2.41	2.37	1.89	1.35
MP2	6-31+G*	2.34	2.40	2.39	2.34	1.88	1.35

		excitation energies of oligomers by TDDFT/eV		
method	basis set	**2Si**	**6Si**$^{+}$	**VD**^{c}
Exp.[d]		6.63		
BH&HLYP	6-31+G*	6.81	2.05	6.68
	6-31+G**	6.80	2.03	6.65
	6-311+G**	6.79	2.02	6.63
B3LYP	6-31+G*	6.12	1.95	6.19

	geometries of polysilane	
method	R_{SiSi}/Å	∠SiSiSi/deg
Exp.[e]	2.37	
BH&HLYP/6-31+G*[f]	2.35	112.9
PBC/PW91 relaxation	2.35	112.7

[a] Reference 1d. [b] R_{SiSi} is the longest bond length and $\overline{R_{SiSi}}$ is the average bond length. [c] **VD** stands for $SiH_3-SiH_2-CH=CH_2$. [d] Reference 17. [e] Reference 24. [f] The values of R_{SiSi} and ∠SiSiSi are adopted from the center part of the **30Si** chain.

interested in the relative difference in excitation energies between polaronized oligomers and the parent ones, 6-31+G* is used in all TDDFT/BH&HLYP calculations for the sake of easier convergence in computations for long oligomers like **30Si**$^{m+}$ ($m = 0-2$).

2.2. Studies of Polymers. Periodic boundary conditions (PBC) were adopted to model infinite chains via repeated unit cells to calculate band structures and densities of states (DOS) of polymers using the DFT method with plane wave basis sets.[18] The functional proposed by Perdew and Wang,[19] named PW91, was applied. The electron−ion interaction was represented by projector-augmented wave (PAW) potentials, which were developed by Kresse, Joubert, and Blöchl.[20] The cutoff energy of plane waves is set to be 250.0 eV. The tetrahedron method with Blöchl corrections[21] is used to determine partial occupancies for setting each wave function. Non-spin-polarized and spin-polarized calculations were carried out for parent and polaronized species, respectively. Computations were performed on an SGI 3800 workstation with the VASP program package,[18] which was developed at the Institut für Theoretische Physik of Technische Universität Wien.

According to the geometries of central portions of oligomers **1**−**4**[22] obtained by BH&HLYP/6-31+G* optimizations, the length L of each unit cell along the polymerization direction (i.e., X direction shown in Figure 2) was determined, and the data are listed in Table 2. Unit cells are then set to be L Å × 15.0 Å × 15.0 Å (X, Y, Z directions, respectively), as exemplified by **PVD** in Figure 2. Each repeated unit includes eight chain atoms for the studied polysilanes. To conveniently describe the extents of charge-doping and heteroatom substitution in a uniform way, we define a doping level, l, in formula (2),

$$l = n_{dopant}/n_{total} \quad (2)$$

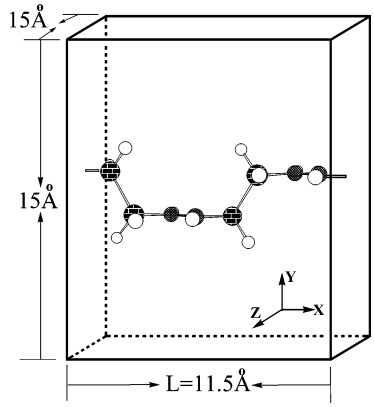

Figure 2. Schematic representations of the unit cell, L Å × 15 Å × 15 Å, of **PVD** for PBC/PW91 calculations. The black, gray, and white balls denote Si, C, and H atoms, respectively.

TABLE 2: Values of L in the Unit Cell of L Å × 15.0 Å × 15.0 Å Setting for PBC/PW91 Calculations

polymer	L/Å
PSi	15.65
charge-doped[a]	15.18
B-substituted (**2a**)[a]	14.62
P-substituted (**2b**)[a]	15.99
PVD	11.50
PBD	16.49

[a] The doping level is $l = 0.125$.

where n_{dopant} and n_{total} refer to numbers of charges (or heteroatoms) and total atoms in a backbone, respectively. Dopants can be either charges in charged oligomers and polymers (e.g., for dications $n_{dopant} = 2$) or heteroatoms in boron- or phosphorus-doped ones (**2**) with $n_{dopant} = 1$ in each repeat unit. For example, in **8Si**$^{+}$ (**1**, $n = 8$, $m = 1$) and charged **PSi** (sharing one charge

over every eight silicon atoms) doping levels are the same, i.e., $l = 1/8 = 0.125$, while for B- and P-substituted polymers **2**, with each unit having one heteroatom and seven silicon atoms, a doping level of $l = 1/8 = 0.125$ is also achieved. Repeated units for $\sigma-\pi$ conjugated polymers **PVD** and **PBD** are set to be $-(SiH_2-SiH_2-CH{=}CH)_2-$ and $-(SiH_2-SiH_2-CH{=}CH-CH{=}CH)_2-$, respectively. The Monkhost−Pack mesh[23] sampling with $21 \times 1 \times 1$ k-point in string Brillouin zone (X, Y, Z directions, respectively) was used. From Table 1 we can find that relaxed structures of polysilane ($R_{SiSi} = 2.35$ Å, ∠SiSiSi $= 112.7°$) based on selected parameters and the conjugate gradient algorithm are in good agreement with BH&HLYP/6-31+G* results ($R_{SiSi} = 2.35$ Å, ∠SiSiSi $= 112.9°$) and experimental observations ($R_{SiSi} = 2.37$ Å).[24] Therefore, results obtained with the above parameters and the PW91 functional in VASP calculations were employed in the following discussions on band structures of σ and $\sigma-\pi$ conjugated polymers.

3. Results and Discussions

We start our discussions from comparisons made between charge-doping and heteroatom substitution on σ conjugated oligosilanes and polysilanes, **1** and **2**. We then elucidate the influence of charge-doping upon $\sigma-\pi$ conjugated chains, **3** and **4**, from which different pictures of σ and $\sigma-\pi$ conjugations are drawn. To simplify our descriptions, we will refer to positive charging in short as charge-doping in the following subsections.

3.1. Charged and Heteroatom-Substituted Oligosilanes and Polysilanes. Experimental X-ray diffraction patterns and absorption and excitation spectra illustrated that silicon backbones mainly take the trans conformation in poly(dimethylsilane)[25] and oligo(dimethylsilane)s $Si_n(Me)_{2n+2}$ ($n = 2-16$).[17,26] Moreover, an all-trans conformation of the radical cation $[Si_n(Me)_{2n+2}]^+$ ($n = 4-18$) was determined by molecular dynamics calculations and PM3-CI optimizations.[10] Therefore, we concentrate our attentions on oligosilanes (by BH&HLYP/6-31+G*) and polysilanes (by PBC/PW91) with all-trans conformations, which may effectively extend σ conjugation in chains.

Conformations. The effects of charge-doping and heteroatom substitution on configurations of oligosilanes can be seen in Figure 3. The original **30Si** takes a slightly twisted conformation, but chains of **30Si**$^+$ and **30Si**$^{2+}$ become straight, implying that charge-doping enhances chain rigidity. Another important feature of charge-doping is that it can noticeably elongate almost all Si−Si bonds (R_{SiSi}) and shrink bond angles (∠SiSiSi) along the **12Si**$^+$ backbone, as shown in Figure 4. The largest distortion, with a lengthening of bonds by 0.032 Å and a narrowing of bond angles by 12.3°, is observed in the central part of the silicon skeleton upon charge-doping (cf. red lines in Figure 4). Such phenomena have also been demonstrated by previous HF and B3LYP calculations[9b,c] on **10Si**$^+$. In fact, after charge-doping, all studied oligomers, ***n*Si**$^{m+}$ ($n = 6-30$, $m = 1,2$), undergo dramatic lengthening of Si−Si bonds and shrinking of bond angles, as reflected by the average bond lengths and bond angles in Table 3.

Furthermore, heavier charge-doping (i.e., with larger values of l) is found to cause even larger distortions with longer R_{SiSi} and smaller ∠SiSiSi than those in singly charged systems. Doping levels of ***n*Si**$^{m+}$ ($n = 6-30$, $m = 1$ or 2) ranging from 0.033 to 0.333 (derived from eq 2) are presented in parentheses in Table 3. There exists a linear relationship between doping level, l, and average bond length, as shown in Figure 5. Here, high doping level l as defined in eq 2 corresponds to two cases: one requires a relatively large amount of charges in a given chain length (i.e., large n_{dopant} and fixed n_{total}), and the other has a fixed number of charges but a shorter backbone (a fixed n_{dopant} and small n_{total}). Thus, charge-doping on a short chain leads to a higher doping level and consequently larger geometry defect than that on a long chain (cf. Table 3 and Figure 5). For example, the average bond length R_{SiSi} is progressively reduced from 2.387 Å (**6Si**$^+$) to 2.353 Å (**30Si**$^+$) with increasing chain length. Radical cations can be stabilized by increasing the chain length, similar to what was suggested for radical anions by Tada and co-workers.[9a] It can be concluded from the above discussion that Si−Si bonds are considerably weakened by charge-doping, especially by doping at a high level. That is the reason why in some experiments cleavages of Si−Si bonds of polysilane have been observed after doping with antimony pentafluoride.[1c]

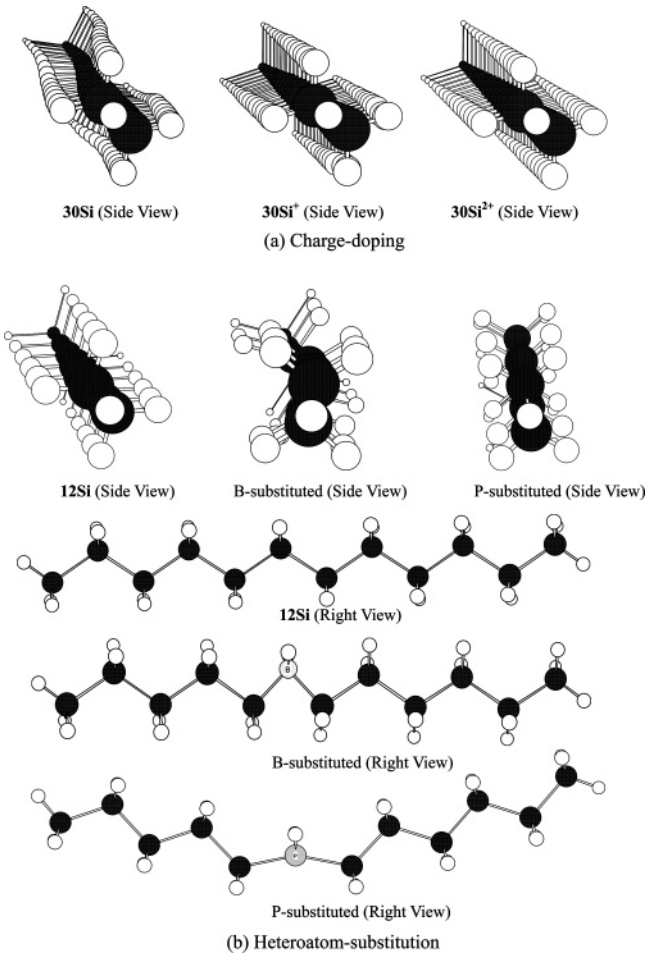

Figure 3. (a) Charge-doping and (b) heteroatom substitution effects on configurations of oligosilanes predicted by (U)BH&HLYP/6-31+G* optimizations. The black and white balls represent Si and H atoms, respectively.

Heteroatom-substituted oligosilanes **2** (at a medium doping level of $l = 0.083$) also undergo obvious chain distortions. In **2**, when there are 11 silicon atoms and one heteroatom X (B or P) in each unit, bond angles of ∠SiXSi (X = B, 88.6°; X = P, 157.3°) are much different from ∠SiSiSi (113.0°) in **1** ($n = 12$, $m = 0$). Such a contracted bond angle of ∠SiBSi and expanded bond angle of ∠SiPSi lead to backbones that are twisted by about 15° and boatlike bending of the chain in the B- and P-substituted oligosilanes, respectively (Figure 3). Covalent Si−B bonds form in B-substituted oligosilane (**2a**) with $R_{SiB} = 2.07$ Å (the documented normal Si−B bond length is 2.07 Å[27]), while in P-substituted **2b** the Si−P bonds ($R_{SiP} = 2.43$ Å) are relatively weaker than standard covalent bonds (R_{SiP}

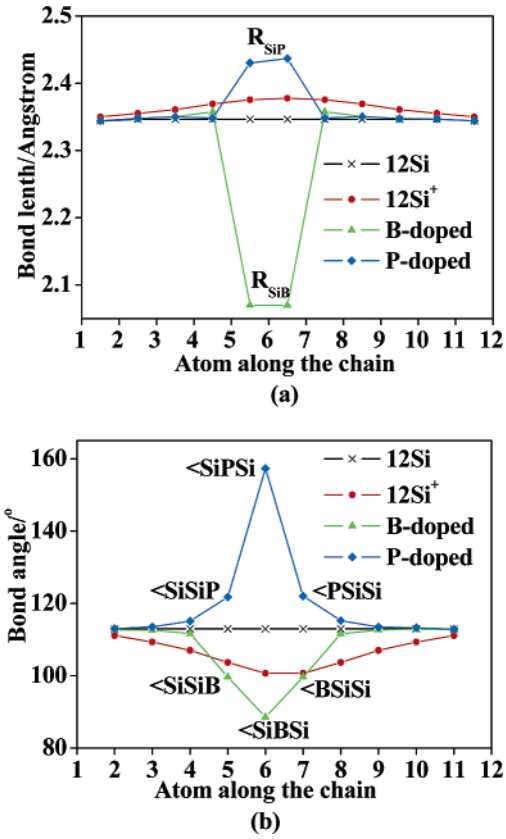

Figure 4. Comparison of (a) bond lengths and (b) bond angles between the charge-doped and heteroatom-substituted oligosilanes.

TABLE 3: Average Bond Lengths, R_{SiSi}, and Bond Angles, ∠SiSiSi, of the Undoped ($m = 0$) and Charge-Doped ($m = 1$ and 2)[a] Oligosilanes Obtained by (U)BH&HLYP/6-31+G* Optimizations

nSi^{m+},	average R_{SiSi}/Å			average ∠SiSiSi/deg		
n	$m = 0$	$m = 1$ (l)	$m = 2$ (l)	$m = 0$	$m = 1$	$m = 2$
6	2.345	2.387 (0.167)	2.431 (0.333)	112.96	99.79	81.13
7	2.346	2.380 (0.143)	2.416 (0.286)	112.92	101.61	86.86
8	2.346	2.374 (0.125)	2.404 (0.250)	112.94	103.01	90.03
9	2.346	2.371 (0.111)	2.403 (0.222)	112.93	104.12	98.62
10	2.346	2.368 (0.100)	2.397 (0.200)	112.95	105.01	100.06
11	2.346	2.365 (0.091)	2.391 (0.182)	112.95	105.76	101.11
12	2.346	2.364 (0.083)	2.387 (0.167)	112.95	106.36	101.97
20	2.346	2.356 (0.050)	2.368 (0.100)	112.96	109.06	105.92
30	2.346	2.353 (0.033)	2.360 (0.066)	112.97	110.41	108.14

[a] Doping levels are given in parentheses.

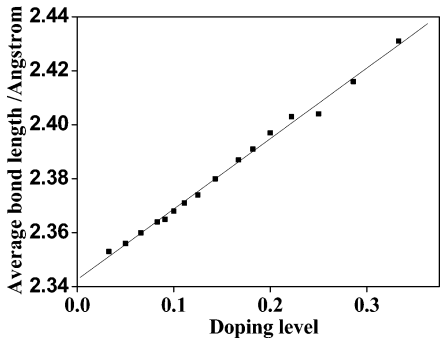

Figure 5. Linear relationship between doping levels, l, and average bond lengths of nSi^{m+} ($n = 6-30$, $m = 1$ or 2).

= 2.27 Å[27]). A comparison of the geometries of charge-doped (**1**) and heteroatom-substituted (**2**) oligosilanes is made in Figure 4. Unlike charge-doping, which induces a relatively larger region of geometric defects, heteroatom substitution exerts only a little influence on neighboring Si−Si bonds around heteroatoms, implying that the bond strength of the backbone is not significantly weakened by B or P substitution. Therefore, heteroatom-substituted polysilanes can be used to design stable conducting materials.

Polarons. It is convenient to describe the existence of a polaron or bipolaron by uneven distributions of spin densities in radical cations or anions. Distributions of spin densities of ground states of selected systems, nSi^{m+} (**1**, $n = 9$, 12, 30; $m = 1$, 2) and **2** ($l = 0.083$), are presented in Figure 6a,b, from which we can schematically describe centers of polarons (also called radicals) along silicon skeletons in Figure 6c by up and down arrows (which represent α and β spins, respectively).

First, we focus on singly charged and heteroatom-substituted oligosilanes. It can be found from Figure 6a that both charge-doping and heteroatom substitution evoke formation of polarons in the middle of oligosilane chains with different extents of dispersion. In **30Si**$^{+}$, the radical (polaron) spreads over a range of about 16 silicon atoms, in agreement with experimental results.[6] In contrast with dispersive polarons in charge-doped oligosilanes, polarons in B- and P-substituted organosilanes are mainly concentrated on small regions of 3−5 atoms. In other words, polarons in heteroatom-substituted oligosilanes are more localized than those in charge-doped ones. Similar to what has been revealed by small defects in heteroatom-substituted chains, the fact that the perturbations on electronic structures caused by B and P substitutions are smaller than those caused by charge-doping also suggests that heteroatom substitution might be a promising strategy to explore potential conducting materials.

We then turn our attention to doubly charged oligosilanes nSi^{2+} ($n = 6-30$). It can be expected that the lowest singlet (S) and triplet (T) states of nSi^{2+} gradually become nearly degenerate with increasing chain length. Table 4 collects energy differences between S and T sates, ΔE_{ST}, of nSi^{2+} ($n = 6-12$, 20, 30). A short chain ($n = 6-10$) prefers a singlet ground state with a negative value of ΔE_{ST}. As the chain grows, the absolute value of ΔE_{ST} gradually approaches zero, implying that degeneracy occurs between the lowest singlet and triplet states. For example, in **10Si**$^{2+}$, the singlet state is lower in energy than the triplet state by 3.64 kcal/mol, while in **30Si**$^{2+}$, the singlet and triplet states become isoenergetic, with zero ΔE_{ST}. In short nSi^{2+} ($n \leq 8$), two charges are stored in the form of spinless bipolarons, as schematically described in Figure 6c. When a chain becomes longer, unpaired electrons with antiparallel spins are localized at the two ends of the backbone, corresponding to formation of two polarons (cf. Figure 6b). For a further elongated chain with up to 30 monomers, two nearly degenerate S and T states demonstrate nearly identical distributions of polarons, except for spins of unpaired electrons (cf. Figure 6b,c). So, we find that doubly charged oligosilanes with long chain length ($n \geq 9$) are beneficial to form two polarons, which facilitates lowering of the band gaps of polysilanes, as verified by the following PBC calculations on polymers.

Band Structures. There are two ways to compute the band gap, E_g, of a polymer: one is to estimate E_g by extrapolating the first optically allowed excitation energies of oligomers to an infinite limit, and the other is to directly evaluate E_g through PBC calculations. Here, we employ both schemes to investigate band structures, and our results are summarized in Table 5. Of course, theoretically predicted band gaps cannot be absolutely compared with those observed experimentally because (1) there may be some uncertainties related to measurements such as

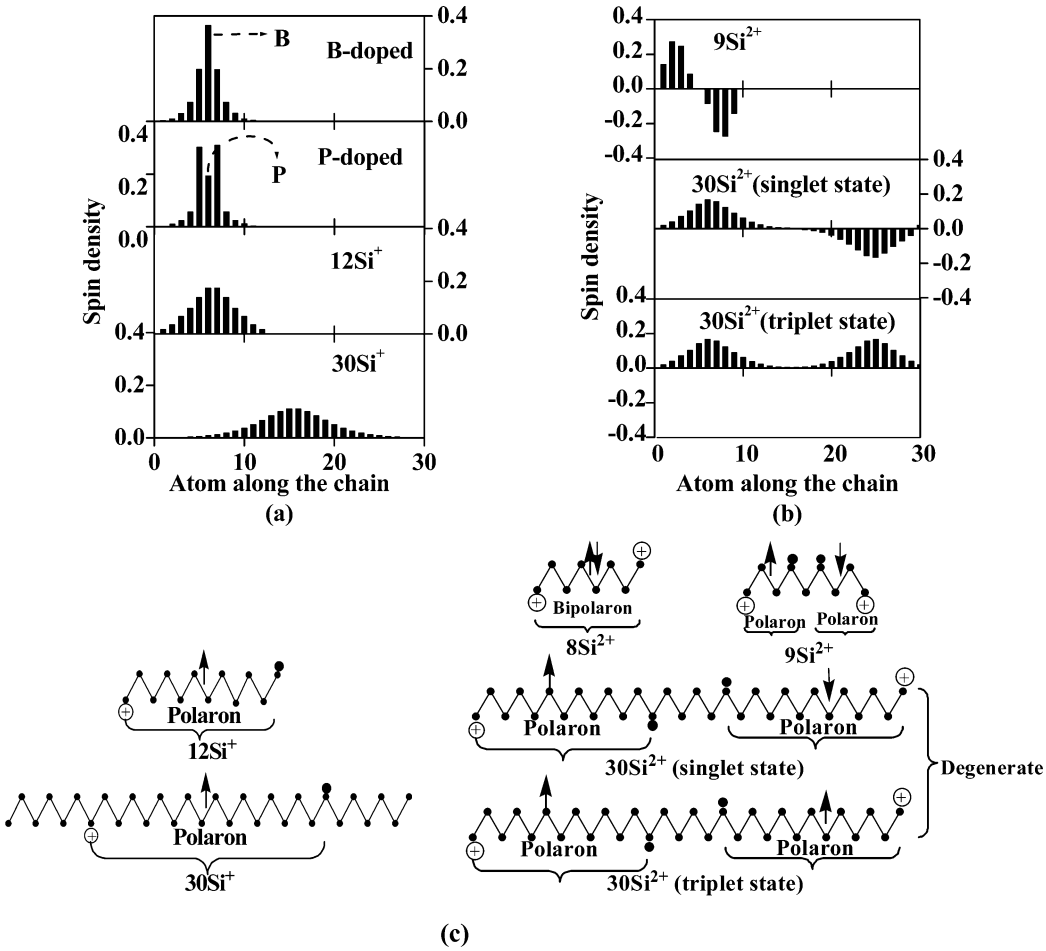

Figure 6. UBH&HLYP/6-31+G* spin density distributions of (a) singly charged and heteroatom-substituted oligosilanes and (b) doubly charged oligosilanes. (c) Descriptions of the polaron and bipolaron of the charge-doped oligosilanes. The zigzag lines represent the skeleton of catenating Si atoms. The polaron and bipolaron bear positive charges, and their representations are referred to ref 3a. The up and down arrows denote the radical centers with the α and β spins, respectively.

TABLE 4: (U)BH&HLYP/6-31+G* Total Energies of nSi^{m+} (n = 6−12, 20, 30; m = 0−2) and Energy Differences, ΔE_{ST}, between Singlet State and Triplet State of Doubly Charged (m = 2) Oligosilanes after Correction by Formula (1)[a]

nSi^{m+},	$m = 0$	$m = 1$	$m = 2$	
n	E_S/au	E_D/au ($\langle S^2\rangle$)	E_S/au ($\langle S^2\rangle$)	ΔE_{ST}/kcal mol^{-1}
6	−1745.2518	−1744.9422 (0.76)	−1744.5110 (0.0)	−12.93
7	−2035.9314	−2035.6267 (0.76)	−2035.2069 (0.0)	−10.40
8	−2326.6110	−2326.3099 (0.76)	−2325.8984 (0.0)	−6.27
9	−2617.2906	−2616.9922 (0.76)	−2616.5893 (0.89)	−5.10
10	−2907.9702	−2907.6738 (0.76)	−2907.2818 (0.94)	−3.64
11	−3198.6498	−3198.3550 (0.76)	−3197.9727 (0.97)	−2.53
12	−3489.3294	−3489.0359 (0.76)	−3488.6620 (0.99)	−1.76
20	−5814.7662	−5814.4769 (0.76)	−5814.1442 (1.02)	−0.04
30	−8721.5623	−8721.2741 (0.76)	−8720.9614 (1.03)	0.00

[a] Values in the parentheses are expectation values of S^2, $\langle S^2\rangle$, to evaluate spin contaminations.

solvent effects, presence of impurities, disorders and defects, etc., and (2) the results may be affected by artificial ideal periodicity, which is necessary for calculations. Despite these challenges, theoretical predictions can still provide qualitative values applicable for a systematic study and give the same trend as experimental determinations.

There exists a good linear correlation between TDDFT excitation energies and experimental spectra of ***n*Si**, as exhibited in Figure 7. The linear relationship is given in eq 3.

$$E_{exp} = 0.55E_{TDDFT} + 1.21 \quad (3)$$

We use eq 3 to calculate corrected excitation energies (as shown in Table 5) by alleviation of systematic errors. Corrected values fit well with experiments, with average deviations of 0.04−0.05 eV. Excitation energies of neutral and charged oligosilanes decrease as a function of number of repeating units, in accord with optical and ESR spectral observations.[4,7,28] Obviously, the band gap of polysilane is significantly lowered by charge-doping. An even−odd effect in charge-doping, as suggested in our previous study on charged π conjugated systems,[29a] is also observed here. For example, the band gap of **PSi**$^{2+}$ (E_g = 0.55 eV) is higher than that of **PSi**$^{+}$ (E_g = 0.16 eV). The understanding of such even−odd effects in π conjugated cations on the basis of the way the band gap splits upon doping, described before,[29a] is also applicable in σ conjugated polysilane cations. In addition, from Table 5 one can notice that charged oligosi-

TABLE 5: Excitation Energies of Oligomers and PBC Results of Polymers

	excitation energies/eV				
	$m = 0, l = 0$			$m = 1$	$m = 2$
oligomers	TDDFT	corr[a]	exptl[b]	TDDFT (l)	TDDFT (l)
***n*Si^{m+} (1)**					
$n = 6$	6.16	4.62	4.68	2.05 (0.167)	4.05 (0.333)
$n = 7$	5.95	4.50	4.52	1.87 (0.143)	3.58 (0.286)
$n = 8$	5.78	4.41	4.40	1.70 (0.125)	3.16 (0.250)
$n = 9$	5.66	4.34	4.31	1.54 (0.111)	1.92 (0.222)
$n = 10$	5.55	4.28	4.22	1.41 (0.100)	1.84 (0.200)
$n = 11$	5.47	4.24		1.30 (0.091)	1.78 (0.182)
$n = 12$	5.40	4.20		1.20 (0.083)	1.71 (0.167)
$n = 20$	5.13	4.05		0.75 (0.050)	1.29 (0.100)
$n = 30$	5.02	3.99		0.46 (0.033)	0.94 (0.066)
$n = \infty$ (E_g)	4.54	3.72	3.76	0.16	0.55
heteroatom-substituted (**2**)					
B-substituted				2.84 (0.083)	
P-substituted				2.87 (0.083)	
$\sigma-\pi$ conjugated oligomers					
3VD^{m+} (3)	5.52			3.30	3.92
3BD^{m+} (4)	4.83			2.31	3.29

	PBC calculations								
						effective masses[c]			
	band gaps, E_g/eV		bandwidths/eV			VB	IB		CB
polymers	PW91	exptl	VB	IB	CB	m_h*	m_e*	m_h*	m_e*
PSi	3.63	3.76[b]	1.52		1.38	0.16			1.02
charge-doped[d]	0.16		0.51	0.57	0.86	0.07	0.04		
B-substituted (**2a**)[d]	1.60		0.32	0.49	0.59	0.07	0.16		
P-substituted (**2b**)[d]	1.23		0.33	0.53	0.47			0.11	0.22
PVD	3.85	4.15[e]	0.61		0.47	0.24			0.19
PBD	3.31		0.21		0.17	0.08			0.07

[a] The corrected TDDFT excitation energies obtained from the work function of formula (3). [b] Reference 28. [c] Units are in mass of a free electron. [d] The doping level is $l = 0.125$. [e] Reference 32.

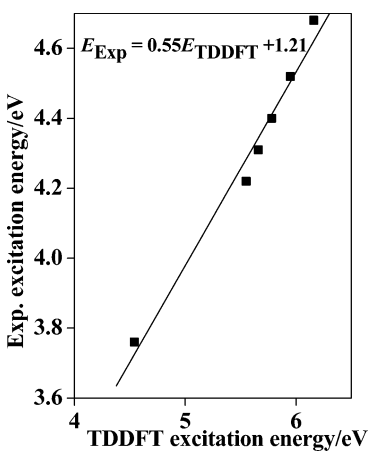

Figure 7. Correlations of TDDFT/BH&HLYP excitation energies at the basis set of 6-31+G* with experimental data for neutral oligosilanes, ***n*Si** ($n = 6-10,\infty$).

lanes with lower doping levels l (i.e., lower concentration of charges) have narrower excitation energies than those with higher doping levels. Furthermore, heteratom substitutions (B-substituted, 2.84 eV; P-substituted, 2.87 eV) decrease excitation energies to a smaller degree than charge-doping (**12Si**$^+$, 1.20 eV) at the same doping level of 0.083 (cf. Table 5).

The above-mentioned effects of charge-doping and heteroatom substitution on excitation energies of oligosilanes ***n*Si** can be understood from qualitative pictures of frontier molecular orbitals. Figure 8 schematically depicts the energy diagram of frontier molecular orbitals and relevant optical transitions of parent, charged, and heteroatom-substituted oligomers. In parent species (***n*Si**), the optical transition comes from the transition

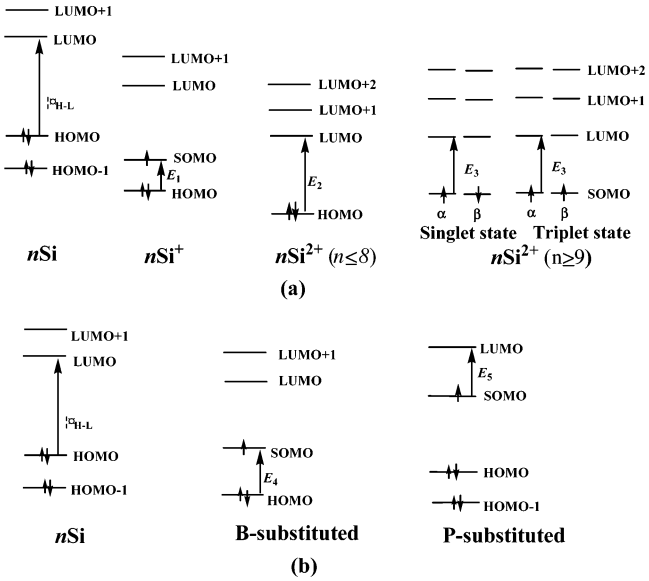

Figure 8. Schematic diagram of frontier molecular orbitals and relevant optical transitions for (a) charge-doped and (b) heteroatom-substituted oligosilanes.

between the highest occupied molecular orbital (HOMO) and the lowest unoccupied molecular orbital (LUMO), as displayed by Δ_{H-L} in Figure 8. With doping by one charge or substitution by a heteroatom (B or P), a singly occupied molecular orbital (SOMO) is formed, splitting the HOMO−LUMO band into two subgaps. TDDFT results show that the first optically allowed transitions of oligosilane cations (***n*Si**$^+$) correspond to a transition from HOMO to SOMO (E_1). When another electron is further

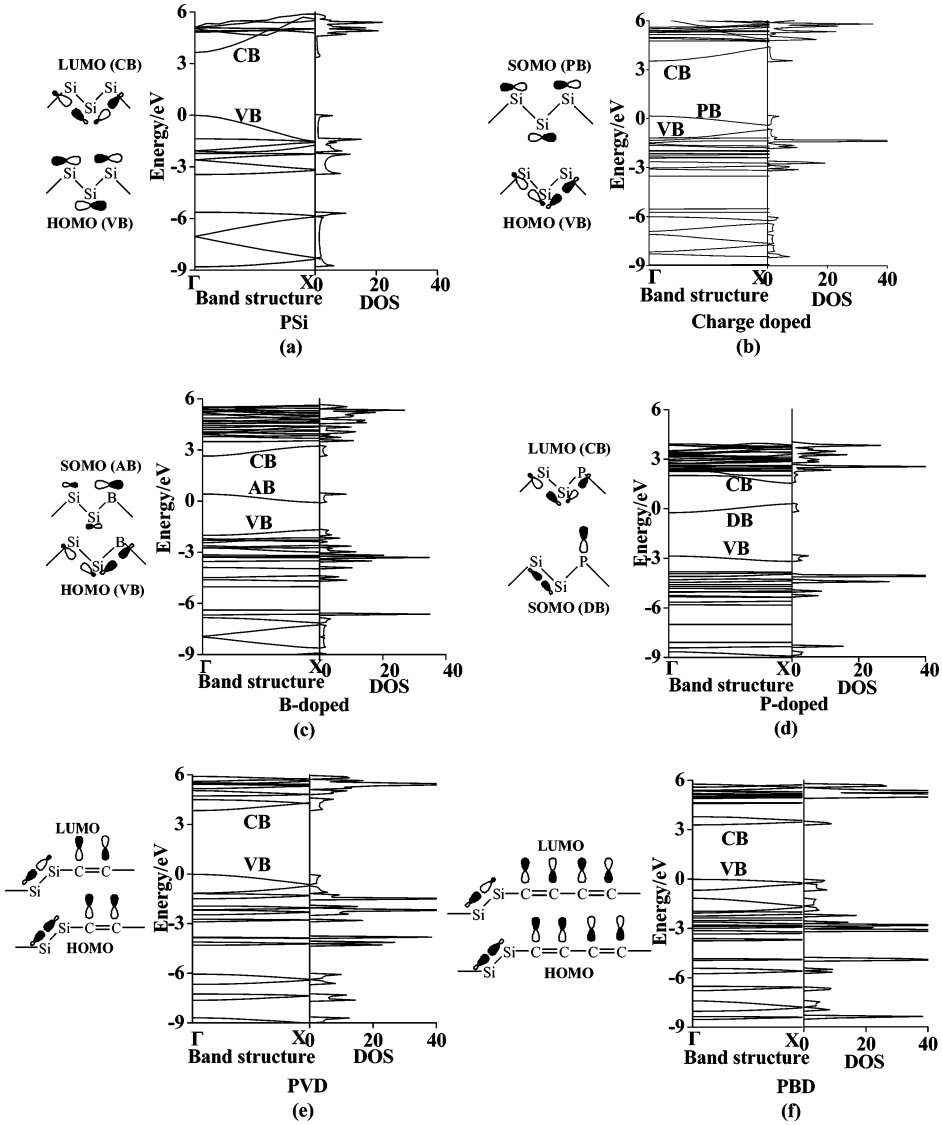

Figure 9. Energy band structures and densities of states (DOS) of the σ and $\sigma-\pi$ conjugated polymers obtained by PBC/PW91 calculations. Orbitals corresponding to the first optically allowed transitions are sketched at the left side. VB, CB, PB, AB, and DB represent for valence, conduction, polaron, acceptor, and donor bands, respectively. The Fermi level is set to be 0.0 eV. The doping level is 0.125.

removed from $n\mathbf{Si}^{+}$, a new lowest vacant orbital, named LUMO, appears. As mentioned before, the formation of bipolarons or polarons in doubly charged oligosilanes depends on chain length, leading to splittings of different subgaps. In short $n\mathbf{Si}^{2+}$ ($n \leq 8$) with bipolaron structures, the first optically allowed transitions correspond to E_2, while in the case of long oligomers of $n\mathbf{Si}^{2+}$ ($n \geq 9$), two SOMOs are formed to accommodate two polarons, respectively, with the first optically allowed transitions corresponding to E_3 between SOMO and LUMO. Similar to the case with singly charged oligosilanes, introduction of a heteroatom (B or P) into the backbone produces a SOMO lying between the HOMO and LUMO, as shown in Figure 8b. The first dipole-allowed transitions in B- and P-substituted oligosilanes are related to HOMO−SOMO (E_4) and SOMO−LUMO (E_5) transitions, respectively. No matter which kind of doping strategy is used, charge-doping or heteroatom substitution, energy gaps between sub-bands (E_1-E_5) are narrower than Δ_{H-L} in parent ones, accounting for the decrease in excitation energies upon introduction of polarons. Moreover, the relatively lower efficiency of reducing the excitation energy by B or P substitution can be also understood on the basis of the different widths of subgaps, as schematically exhibited in Figure 8.

From oligomers to polymers, orbital levels integrate into bands, so it is also useful to study the effects of charge-doping and heteroatom substitution on band structures of polysilanes. From Table 5, it can be found that the band gap (E_g) of the parent polysilane calculated by PBC/PW91 (3.63 eV) is in better agreement with experimental value (3.76 eV) than the extrapolated TDDFT band gap (4.54 eV). The improved performance of PBC/PW91 calculations may be attributed to both the PW91 functional and elimination of boundary effects by PBC treatment. Obviously, charge-doping (at a doping level $l = 0.125$), B substitution, and P substitution ($l = 0.125$) considerably lower the band gap of polysilane to 0.16, 1.60, and 1.23 eV, respectively. Again, charge-doping is shown to reduce the band gap more significantly than B or P substitution.

Figure 9 gives band structures and densities of states (DOS) for parent (Figure 9a), charged (Figure 9b with $l = 0.125$), B-substituted (Figure 9c), and P-substituted (Figure 9d) polysilanes, with related orbitals sketched beside the band structures. The calculated band gaps, bandwidths, and effective masses of electrons (m_e*) and holes (m_h*) at band edges are presented in Table 5. Both parent and polaronized linear polysilanes have directly allowed band structures, in contrast

TABLE 6: Interaction Energy between Electron-Donating (Bonding σ_{SiSi} or Lone Pair n_P) and Electron-Accepting (Antibonding σ_{SiSi}* and Vacant p_B) Orbitals, ΔE/kJ mol^{-1}, Obtained by Natural Bond Orbital Analysis

Species	Orbital Interaction Energy, ΔE/kJ.mol^{-1}		
	$\sigma \rightarrow \sigma^*$	$\sigma \rightarrow p$	$n \rightarrow \sigma^*$
12Si	0.8		
12Si$^+$		25.0 ($\sigma_{SiSi} \rightarrow p_{Si}$)	
B-substituted		21.0 ($\sigma_{SiSi} \rightarrow p_B$)	
P-substituted			15.2 ($n_P \rightarrow \sigma_{SiSi}^*$)

to the indirect semiconducting property of unpolaronized bulk Si.[30] It is well known that charge-doping and heteroatom substitution can introduce an half-filled impurity band (IB) (close to the Fermi level of 0.0 eV) between the valence band (VB) and the conduction band (CB). The IBs resulting from charge-doping, B substitution, and P substitution are, respectively, a polaron band (PB) constructed from p_x orbitals (σ-type) of Si atoms, an acceptor band (AB) mainly coming from p_x orbitals of B atoms, and a donor band (DB) originating from p_y orbitals of P atoms. The transition, either from VB to PB (or AB) or from DB to CB, corresponds to a lowering of the band gaps of polysilanes upon charge-doping, B substitution, and P substitution (cf. Table 5). In charged or heteroatom-substituted polymers, not only does IB have a small bandwidth (around 0.5 eV), but also the bandwidths of VB and CB (0.3−0.8 eV) become narrower than those of the parent **PSi** (1.4−1.5 eV) (as shown in Table 5). In addition, charge-doping and heteroatom substitution not only lower effective masses of electrons (m_e*) and holes (m_h*) at the VB and CB band edges, but also produce small m_e* and m_h* at the IB band edge. These phenomena indicate that both charge-doping and heteroatom substitution can increase the conductivity of **PSi**. The decrease in effective masses after charge-doping and heteroatom substitution may also reflect an enhancement of conjugation effects, which will be discussed below.

Conjugation Effects. It is well recognized that band gaps correlate closely with amounts of conjugation in both σ and π conjugated systems. The extent of conjugation can be reflected by bond orbital interaction between an electron-donating orbital (such as the σ_{SiSi} bonding orbital or the lone pair orbital n_p of the P atom) and an electron-accepting orbital (e.g., an empty antibonding orbital, σ_{SiSi}*, or a vacant p_B orbital of the B atom) of its vicinal bond. Here, natural bond orbital (NBO) analysis[31] is employed to estimate the magnitude of the conjugation effect. Interaction energies between electron donors and acceptors are shown in Table 6. As expected, both charge-doping and heteroatom substitution significantly increase the amount of conjugation. Pronounced interactions of $\sigma \rightarrow$p (for charged and B-substituted) and n$\rightarrow\sigma$* (for P-substituted) reveal strong electron−hole interactions, which is essential for lowering of band gaps and floating of charge carriers with small m_e* and m_h* under electron fields.

3.2. Cations of $\sigma-\pi$ Conjugated Chains. Oligomers and polymers containing $\sigma-\pi$ conjugated moieties, such as ***n*VD** [**3**, $-(SiH_2SiH_2CH{=}CH)_n-$], and ***n*BD** [**4**, $-(SiH_2SiH_2CH{=}CH{-}CH{=}CH)_n-$], and especially their doped counterparts, are much less studied than those with purely σ or π conjugated units. In this subsection, we investigate differences in electronic structures between cations of $\sigma-\pi$ conjugated systems and σ conjugated polysilanes.

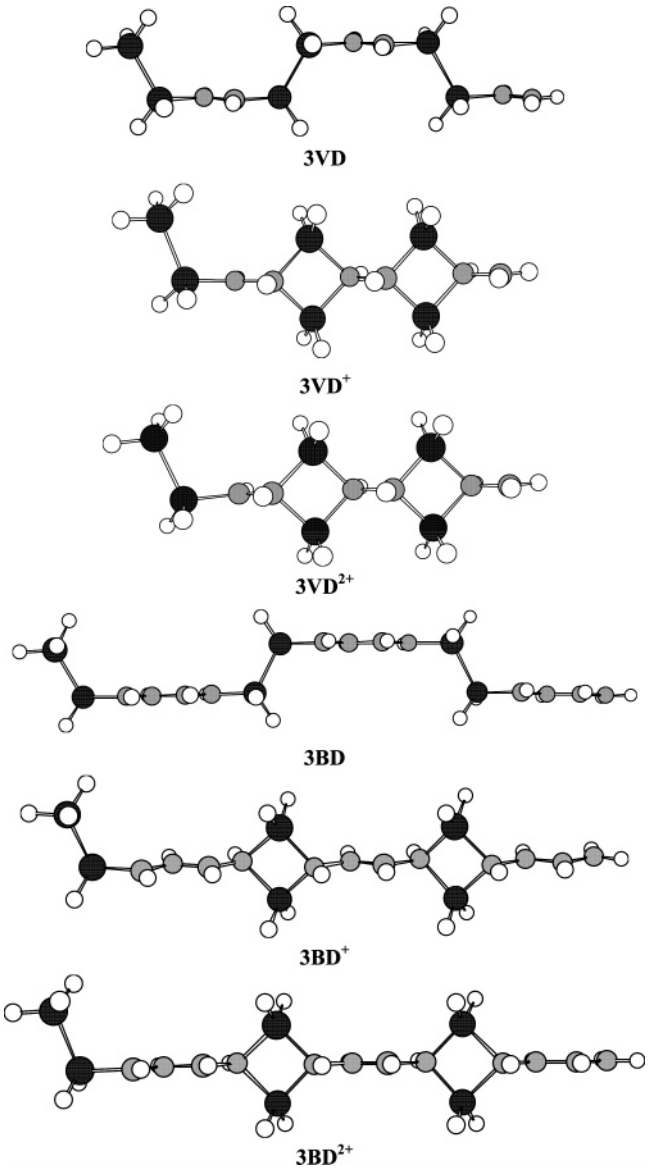

Figure 10. Most stable structures of the doped and undoped $\sigma-\pi$ conjugated oligomers obtained by BH&HLYP/6-31+G* optimizations. The black, gray, and white balls denote Si, C, and H atoms, respectively.

Bridged Structures Formed by Charge-Doping. By searching for possible configurations (cf. Figure S2 and Table S1 in the Supporting Information), we find that the most stable conformers of **3VD** and **3BD** are the cis-skew conformations (Figure 10). Interestingly, after charge-doping, the most stable structures of **3VD^{m+}** and **3BD^{m+}** ($m = 1, 2$) turn to bridged ones, which are also presented in Figure 10. Four atoms in each bridged structure in **3VD^{m+}** and **3BD^{m+}** ($m = 1, 2$) are coplanar. Other less stable conformers of **3VD^{m+}** and **3BD^{m+}** ($m = 1, 2$) are presented in Figure S3 of the Supporting Information, with their relative energies given in Table S2.

Analogous to those in σ conjugated chains, all bonds (including Si−Si and Si−C bonds) of **3VD** and **3BD** are also elongated by charge-doping (cf. Tables S3 and S4 in the Supporting Information). Formations of bridged structures in **3VD^{m+}** and **3BD^{m+}** leads to transformations of hybridizations on carbon atoms from sp^2 (in the neutral state) to sp^3 (in cations). In comparison with those in neutral **3VD**, carbon−carbon bond lengths in **3VD$^+$** and **3VD^{2+}** are elongated by 0.03−0.2 Å. For π conjugated systems, charge-doping changes the extent of alternations in bond length, δ, which is an important index to

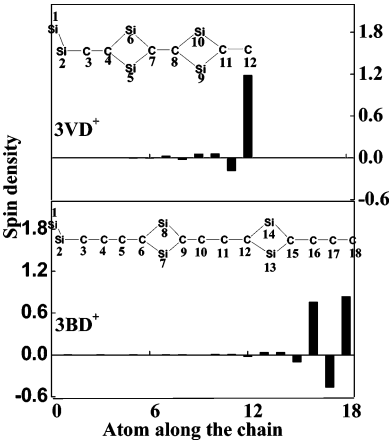

Figure 11. UBH&HLYP/6-31+G* spin densities of singly charged $\sigma-\pi$ conjugated oligosilanes, **3VD**$^+$ and **3BD**$^+$. Only the skeleton atoms are listed and labeled here for simplicity.

measure the amount of π conjugation. Average values of δ are reduced from 0.12 Å in **3BD** to 0.04−0.05 Å in **3BD**$^+$ and to 0.02−0.05 Å in **3BD**$^{2+}$, suggesting that delocalization of π electrons is enhanced.

Location of Polarons and Bipolarons. Distributions of spin density in singly charged **3VD**$^+$ and **3BD**$^+$ are shown in Figure 11, from which polarons are found to be trapped in terminal π conjugated moieties. Doubly charged $\sigma-\pi$ conjugated chains have singlet ground states, with the lowest singlet states of **3VD**$^{2+}$ and **3BD**$^{2+}$ lying 50.35 and 39.56 kcal mol^{-1} below the lowest triplet states, respectively (cf. Table S2 in the Supporting Information). In other words, in contrast to ***n*Si**$^{2+}$ ($n \geq 9$), two injected charges prefer to form spinless bipolarons in **3VD**$^{2+}$ and **3BD**$^{2+}$. Formation of polarons and bipolarons in **3VD**$^{m+}$ and **3BD**$^{m+}$ ($m = 1$ and 2) is expected to decrease the excitation energies of $\sigma-\pi$ conjugated systems. As demonstrated from Table 5, for examples, the excitation energies of **3VD**$^+$ and **3BD**$^+$ are 2.22 and 2.52 eV lower than those of **3VD** and **3BD**, respectively.

Band Structures. The π conjugated moiety in a $\sigma-\pi$ conjugated chain is demonstrated to play an important role in lowering the band gap (cf. Table 5 and Figure 9e,f). In each repeating cell of **PBD**, two successively π conjugated units (C=C) are inserted into the Si−Si unit, while the **PVD** cell has a σ/π alternating alignment. From Table 5, one can find that the band gap of **PBD** (3.31 eV) is lower than those of **PVD** (3.85 eV) and **PSi** (3.63 eV). Furthermore, the effective mass of a hole of **PBD** ($m_h^* = 0.08m_0$) is smaller than those of **PVD** ($0.24m_0$) and **PSi** ($0.16m_0$), implying that the hole conductivity of **PBD** (**4**) may be more effective than those of **PVD** (**3**) and **PSi** (**1**). Therefore, **PBD**, with a low band gap, is suggested to be a promising candidate for synthesis.

4. Conclusions

The effects of charge-doping and boron and phosphorus substitution on the electronic structures and band gaps of σ and $\sigma-\pi$ conjugated systems, **1**−**4**, have been theoretically investigated by using density functional theory and time-dependent density functional theory. Band gaps of the polymers were estimated by both extrapolations from TDDFT excitation energies of oligomers with up to 30 monomers and PBC calculations. It has been found that charge-doping on polysilane decreases the band gap more significantly than B and P substitutions. However, Si−Si bonds are easily broken in charged polysilanes. In contrast, B and P substitutions exert little influence on the strength of Si−Si bonds.

The lowering of band gaps upon charge-doping or heteroatom substitution was ascribed to formation of polarons or bipolarons. A polaron in singly charged polysilane was demonstrated to spread over a region of about 16 Si atoms, in agreement with experimental observations. The two injected charges in doubly charged oligosilane with long chain length ($n \geq 9$) tend to form two localized polarons at the two ends. The band gap of polysilane is significantly reduced from 3.63 eV to 0.16, 1.60, and 1.23 eV by charge-doping, B substitution, and P substitution, respectively, at the same doping level of $l = 0.125$. Natural bond orbital (NBO) analysis was applied to study the effects of charge-doping and heteroatom substitution on the extent of electron delocalization. It was concluded that charge-doping and heteroatom substitution bring about a lowering of the band gap in σ conjugated polysilanes because of strong electron−hole interactions.

Furthermore, it has been demonstrated that π conjugated moieties play an important role in tuning the electronic structures of $\sigma-\pi$ conjugated chains, ***n*VD** (**3**) and ***n*BD** (**4**). The introduction of longer π conjugated moieties in $\sigma-\pi$ conjugated chains can reduce band gaps. In contrast to the case with σ conjugated oligosilanes, bridged structures of **3VD**$^{m+}$ and **3BD**$^{m+}$ (m=1−2) are formed upon charge-doping with the polaron trapped in terminal π conjugated moieties.

Acknowledgment. China NSF (Nos. 90303020, 20420150034, and 20433020) is thanked for financial support.

Supporting Information Available: Geometries and energies of various configurations of **VD**, **BD**, **3VD**$^{m+}$, and **3BD**$^{m+}$ ($m = 0-2$) obtained by BH&HLYP/6-31+G*calculations; spin densities of **30Si**$^+$ obtained by BH&HLYP/6-31+G* and B3LYP/6-31+G* calculations. This material is available free of charge via the Internet at http://pubs.acs.org.

References and Notes

(1) (a) Koshida, N.; Matsumoto, N. *Mater. Sci. Eng., R* **2003**, *40*, 169−205. (b) Hayase, S. *Prog. Polym. Sci.* **2003**, *28*, 359−381. (c) Ishikawa, M.; Ohshita, J. In *Handbook of Organic Conductive Molecules and Polymers*, Vol. 2; Nalwa, H. S., Ed.; John Wiley & Sons: New York, 1997; pp 685−717. (d) Miller, R. D.; Michl, J. *Chem. Rev.* **1989**, *89*, 1359−1410. (e) West, R. *J. Organomet. Chem.* **1986**, *300*, 327−346.

(2) (a) Zeng, X. B.; Liao, X. B.; Wang, B.; Dai, S. T.; Xu, Y. Y.; Xiang, X. B.; Hu, Z. H.; Diao, H. W.; Kong, G. L. *J. Crystal Growth* **2004**, *265*, 94−98. (b) Cui, Y.; Lieber, C. M. *Science* **2001**, *291*, 851−853. (c) Holmes, J. D.; Johnston, K. P.; Doty, R. C.; Korgel, B. A. *Science* **2000**, *287*, 1471−1473. (d) Cui, Y.; Duan, X.; Hu, J.; Lieber, C. M. *J. Phys. Chem. B* **2000**, *104*, 5213−5216. (e) Morales, A. M.; Lieber, C. M. *Science* **1998**, *279*, 208−211.

(3) (a) Kertesz, M. In *Handbook of Organic Conductive Molecules and Polymers*, Vol. 4; Nalwa, H. S., Ed.; John Wiley & Sons: New York, 1997; pp 147−172. (b) Roncali, J. *Chem. Rev.* **1997**, *97*, 173−205. (c) Hong, S. Y.; Marynick, D. S. *J. Chem. Phys.* **1992**, *96*, 5497.

(4) (a) Rice, M. J.; Phillpot, S. R. *Phys. Rev. Lett.* **1987**, *58*, 937−940. (b) Brédas, J. L.; Cornil, J.; Beljonne, D.; Dos Santos, D. A.; Shuai, Z. *Acc. Chem. Res.* **1999**, *32*, 267−276.

(5) Van Haare, J. A. E. H.; Havinga, E. E.; Van Dongen, J. L. J.; Janssen, R. A. J.; Cornil, J.; Brédas, J. L. *Chem. Eur. J.* **1998**, *4*, 1509−1522.

(6) Irie, S.; Irie, M. *Macromolecules* **1997**, *30*, 7906−7909.

(7) Kumagai, J.; Yoshida, H.; Ichikawa, T. *J. Phys. Chem.* **1995**, *99*, 7965−7969.

(8) Irie, S.; Irie, M. *Macromolecules* **1992**, *25*, 1766−1770.

(9) (a) Tada, T.; Yoshimura, R. *J. Phys. Chem. A* **2003**, *107*, 6091−6098. (b) Toman, P.; Nešpůrek, S.; Jang, J. W.; Lee, C. E. *Curr. Appl. Phys.* **2002**, *2*, 327−330. (c) Toman, P. *Synth. Met.* **2000**, *109*, 259−261.

(10) Tachikawa, H. *Chem. Phys. Lett.* **1997**, *265*, 455−459.

(11) (a) Seki, S.; Kunimi, Y.; Nishida, K.; Yoshida, Y.; Tagawa, S. *J. Phys. Chem. B* **2001**, *105*, 900−904. (b) Seki, S.; Yoshida, Y.; Tagawa, S. *Radiat. Phys. Chem.* **2001**, *60*, 411−415. (c) Seki, S.; Yoshida, Y.; Tagawa, S.; Asai, K. *Macromolecules* **1999**, *32*, 1080−1086. (d) Ichikawa, T.; Kumagai, J.; Koizumi, H. *J. Phys. Chem. B* **1999**, *103*, 3812−3817.

(12) (a) Ohshita, J.; Hashimoto, M.; Lee, K. H.; Yoshida, H.; Kunai, A. *J. Organomet. Chem.* **2003**, *682*, 267−271. (b) Hayashi, T.; Uchimaru, Y.; Reddy, N. P.; Tanaka, M. *Chem. Lett.* **1992**, 647−650. (c) Ohshita, J.; Kanaya, D.; Ishikawa, M.; Koike, T.; Yamanaka, T. *Macromolecules* **1991**, *24*, 2106−2107. (d) Ishikawa, M.; Hasegawa, Y.; Kunai, A.; Yamanaka, T. *J. Organomet. Chem.* **1990**, *381*, C57−C59. (e) Ohshita, J.; Kanaya, D.; Ishikawa, M.; Yamanaka, T. *J. Organomet. Chem.* **1989**, *369*, C18−C20.

(13) Frisch, M. J.; Trucks, G. W.; Schlegel, H. B.; Scuseria, G. E.; Robb, M. A.; Cheeseman, J. R.; Zakrzewski, V. G.; Montgomery, J. A., Jr.; Stratmann, R. E.; Burant, J. C.; Dapprich, S.; Millam, J. M.; Daniels, A. D.; Kudin, K. N.; Strain, M. C.; Farkas, O.; Tomasi, J.; Barone, V.; Cossi, M.; Cammi, R.; Mennucci, B.; Pomelli, C.; Adamo, C.; Clifford, S.; Ochterski, J.; Petersson, G. A.; Ayala, P. Y.; Cui, Q.; Morokuma, K.; Salvador, P.; Dannenberg, J. J.; Malick, D. K.; Rabuck, A. D.; Raghavachari, K.; Foresman, J. B.; Cioslowski, J.; Ortiz, J. V.; Baboul, A. G.; Stefanov, B. B.; Liu, G.; Liashenko, A.; Piskorz, P.; Komaromi, I.; Gomperts, R.; Martin, R. L.; Fox, D. J.; Keith, T.; Al-Laham, M. A.; Peng, C. Y.; Nanayakkara, A.; Challacombe, M.; Gill, P. M. W.; Johnson, B.; Chen, W.; Wong, M. W.; Andres, J. L.; Gonzalez, C.; Head-Gordon, M.; Replogle, E. S.; Pople, J. A. *Gaussian 98*, Revision A.11; Gaussian, Inc.: Pittsburgh, PA, 2001.

(14) (a) Cremer, D.; Filatov, M.; Polo, V.; Kraka, E.; Shaik, S. *Int. J. Mol. Sci.* **2002**, *3*, 604−638. (b) Gräfenstein, J.; Kraka, E.; Filatov, M.; Cremer, D. *Int. J. Mol. Sci.* **2002**, *3*, 360−394. (c) Becke, A. D. *J. Chem. Phys.* **1993**, *98*, 1372−1377.

(15) Cremer, D. *Mol. Phys.* **2001**, *99*, 1899−1940.

(16) (a) Takano, Y.; Kubo, S.; Onishi, T.; Isobe, H.; Yoshioka, Y.; Yamaguchi, K. *Chem. Phys. Lett.* **2001**, *335*, 395−403. (b) Soda, T.; Kitagawa, Y.; Onishi, T.; Takano, Y.; Shigeta, Y.; Nagao, H.; Yoshioka, Y.; Yamaguchi, K. *Chem. Phys. Lett.* **2000**, *319*, 223−230. (c) Yamaguchi, K.; Jensen, F.; Dorigo, A.; Houk, K. N. *Chem. Phys. Lett.* **1988**, *149*, 537−542.

(17) Plitt, H. S.; Balaji, V.; Michl, J. *Chem. Phys. Lett.* **1993**, *213*, 158−162.

(18) (a) Kresse, G.; Furthmüller, J. *Comput. Mater. Sci.* **1996**, *6*, 15−50. (b) Kresse, G.; Furthmüller, J. *Phys. Rev. B* **1996**, *54*, 11169−11185.

(19) Perdew, J. P.; Chevary, J. A.; Vosko, S. H.; Jackson, K. A.; Pederson, M. R.; Singh, D. J.; Fiolhais, C. *Phys. Rev. B* **1992**, *46*, 6671−6687.

(20) (a) Kresse, G.; Joubert, D. *Phys. Rev. B* **1999**, *59*, 1758−1775. (b) Blöchl, P. E. *Phys. Rev. B* **1994**, *50*, 17953−17979.

(21) Blöchl, P. E.; Jepsen, O.; Andersen, O. K. *Phys. Rev. B* **1994**, *49*, 16223−16233.

(22) For **1**, the geometry of the oligomer with $n = 30$ is adopted; for **2**, $n_1 = 5$, $n = 6$; and for both **3** and **4**, $n = 3$ is taken.

(23) Monkhorst, H. J.; Pack, J. D. *Phys. Rev. B* **1976**, *13*, 5188−5192.

(24) McCrary, V. R.; Sette, F.; Chen, C. T.; Lovinger, A. J.; Robin, M. B.; Stöhr, J.; Zeigler, J. M. *J. Chem. Phys.* **1988**, *88*, 5925−5933.

(25) Furukawa, S. *J. Organomet. Chem.* **2000**, *611*, 36−39.

(26) Raymond, M. K.; Michl, J. *Int. J. Quan. Chem.* **1999**, *72*, 361−367.

(27) Stark, J. G.; Wallace, H. G. *Chemistry Data Book*; John Murray: London, 1975; p 32.

(28) Obata, K.; Kira, M. *Organometallics* **1999**, *18*, 2216−2222.

(29) (a) Zhang, G.; Ma, J.; Jiang, Y. *Macromolecules* **2003**, *36*, 2130−2140. (b) Ma, J.; Li, S.; Jiang, Y. *Macromolecules* **2002**, *35*, 1109−1115.

(30) Brus, L. *J. Phys. Chem.* **1994**, *98*, 3575−3581.

(31) Reed, A. E.; Curtiss, L. A.; Weinhold, F. *Chem. Rev.* **1988**, *88*, 899−926.

(32) Mercuri, F.; Sgamellotti, N.; Re, A. *J. Mol. Struct. (THEOCHEM)* **1999**, *489*, 35−41.